EDN: EFCEHY
УДК 535.34; 544.47

Solid-phase Synthesis and Photocatalytic Properties of $Bi_2SiO_5/Bi_{12}SiO_{20}$ Heterostructures

Aleksandra G. Golubovskaya*
Tamara S. Kharlamova†
Valery A. Svetlichnyi‡
Tomsk State University
Tomsk, Russian Federation

Received 29.10.2024, received in revised form 13.12.2024, accepted 24.01.2025

Abstract. In this work, a new approach to the preparation of heterostructured nanoparticles (NPs) based on bismuth silicates $Bi_2SiO_5/Bi_{12}SiO_{20}$ is proposed and implemented. This approach is based on solid-phase synthesis by annealing of a pre-homogenized mixture of β-Bi_2O_3 and SiO_2 powders in different ratios. For this purpose, industrial silica nanopowder and β-bismuth oxide NPs powder obtained by pulsed laser ablation (PLA) in air are used. The morphology, phase composition and optical properties of the obtained materials are studied. By changing the ratio of precursors, the powders similar in structure to single-phase bismuth silicates Bi_2SiO_5 and $Bi_{12}SiO_{20}$ as well as heterostructured NPs on their basis are obtained. The activity of the photocatalysts in the reactions of Rhodamine B (Rh B) decomposition and selective oxidation of 5-hydroxymethylfurfural (5-HMF) is estimated. The best photocatalytic activity is demonstrated by powders with a similar $Bi_2SiO_5/Bi_{12}SiO_{20}$ (or 4Bi: 1Si) phase ratio. As a result of the analysis of the data obtained, the formation of a type II heterojunction is proposed.

Keywords: solid-phase synthesis, bismuth silicates, heterostructured nanoparticles, pulsed laser ablation, photocatalysis, heterojunction II type, rhodamine B, 5-hydroxymethylfurfural.

Citation: A.G. Golubovskaya, T.S. Kharlamova, V.A. Svetlichnyi, Solid-phase Synthesis and Photocatalytic Properties of $Bi_2SiO_5/Bi_{12}SiO_{20}$ Heterostructures, J. Sib. Fed. Univ. Math. Phys., 2025, 18(3), 309–319. EDN: EFCEHY.

Introduction

In recent years, photocatalytic (PC) technologies have attracted increasing interest due to their great potential for solving challenges in green energy, bioresource processing, and ecology [1–3] Photocatalysis is effective for cleaning the industrial wastewater from synthetic dyes, phenols, and antibiotics [4]. Another promising area of photocatalysis is the production of valuable materials with high added value by oxidizing intermediate products of processing of biomass, the most accessible raw material on Earth [5]. For instance, selective photooxidation of 5-hydroxymethylfurfural (5-HMF) can produce 5-formyl-2-furancarboxylic acid (FFCA) and subsequently 2,5-furandicarboxylic acid (FDCA) [6]. The FFCA and FDCA are an alternative substitute for phthalic acid and furan polymers, which are obtained from fossil resources and are

*aleksandra.golubovskaya@mail.ru https://orcid.org/0000-0002-9273-1825
†kharlamova83@gmail.com https://orcid.org/0000-0002-6463-3582
‡v_svetlichnyi@bk.ru https://orcid.org/0000-0002-3935-0871

widely used in industry. The ability to use sunlight as a radiation source and non-toxic, low-cost materials as catalysts makes photocatalysis a safe and environmentally friendly method.

The effectiveness of PC technologies primarily depends on the catalyst characteristics. Currently, the most successful and promising photocatalysts are materials based on semiconductor nanoparticles (NPs). Due to a wide choice of semiconductor materials, it is possible to select a photocatalyst with the desired value of the band gap (E_g) for optimal light absorption. The use of NPs as photocatalysts is due to their unique physical-chemical properties, including size, morphology, surface charge, large specific surface area, spectroscopic characteristics, and the presence of defects. Among the wide variety of photocatalysts, bismuth-based materials are distinguished [7, 8], in particular bismuth silicates (Bi_2SiO_5, $Bi_{12}SiO_{20}$) [9, 10], which feature suitable physical-chemical properties. However, as in the majority of single-phase semiconductors, a relatively rapid charge recombination occurs in bismuth silicates, which reduces their PC activity [11]. The best solution to this problem is currently considered to be the creation of heterostructured NPs consisting of two or more semiconductors with different band gaps. If the heterojunction is of the so-called type II, then spatial charge separation occurs better in such a composite particle. If the Z-scheme of operation is implemented in NPs based on such a heterojunction, then it is also possible to increase the oxidation-reduction capacity of the photocatalyst [12, 13].

An important task in the development of the PC technologies is the elaboration of methods to synthesize new photocatalysts. It is possible to increase the variability and effectively control the structure and properties of materials by combining different synthesis methods. This approach also allows one to avoid the limitations inherent in any single method. For instance, along with traditional chemical synthesis approaches, the laser methods to synthesize the nanomaterials for photocatalysis have recently been actively developed [14, 15]. Thus, by combining procedures such as pulsed laser ablation (PLA), laser treatment (LT) of colloids, coprecipitation, drying and annealing, various single-phase and composite particles based on bismuth oxides and silicates were obtained [16, 17].

In this work, a new approach to prepare the heterostructured NPs of bismuth silicates $Bi_2SiO_5/Bi_{12}SiO_{20}$ was proposed. The approach was based on solid-phase synthesis by annealing a pre-homogenized mixture of β-Bi_2O_3 and SiO_2 powders in different ratios by grinding. In this case, β-bismuth oxide powder obtained by PLA in air was used as one of the precursors. The structure and properties of the obtained powders as well as their PC activity in the reactions of Rhodamine B (Rh B) decomposition and selective oxidation of 5-HMF were studied and analyzed.

1. Materials and methods

The samples were obtained by the solid-phase synthesis from precursors, namely, SiO_2 and β-Bi_2O_3 nanopowders. The β-Bi_2O_3 powder was obtained by PLA of metallic bismuth (99.5 % purity) in atmospheric air. Ablation was carried out by focusing radiation of the LS2131-20 Nd:YAG laser (LOTIS TII, Belarus) (1064 nm, 7 ns, 150 mJ, 20 Hz) onto the target. The laser power density on the target surface was 1200 MW/cm^2. The nanopowder obtained as a result of the PLA consisted predominantly of the β-bismuth oxide phase ($\sim$94 %, with an admixture of non-stoichiometric bismuth oxide) with an average particle size of 20 nm and a specific surface area of 44 m^2/g. The experimental technique and powder characteristics are described in detail in Ref. [18]. Silica of the Polysorb MP brand (JSC "Polysorb", Russia) had a particle size of less

than 10 nm and a specific surface area of 300 m^2/g.

Bismuth and silicon oxides were mixed at atomic ratios Bi:Si = 2:1, 4:1, 6:1, 8:1, 12:1. The extreme ratios in this series correspond to stoichiometric Bi_2SiO_5 and $Bi_{12}SiO_{20}$ bismuth silicates. The mixtures were then thoroughly ground in an agate mortar for 15 min. The resulting series of samples was calcined at 600 °C in a muffle furnace for 4 h.

The size and shape of the NPs were analyzed using the CM12 transmission electron microscope (Philips, Netherlands). The crystal structure of the powders was studied by X-ray diffraction using the XRD 6000 diffractometer (Shimadzu, Japan). The phase content was analyzed using the Powder Diffraction Database PDF-4 (ICDD, USA) and PowderCell 2.4 software. The optical properties of the powders were studied by diffuse reflectance spectroscopy (DRS) in the UV-Vis range using the Cary 100SCAN spectrophotometer (Varian, Australia) with the DRA-CA-30I add-on (Labsphere, USA). The band gap (E_g) was estimated using two methods. The widely used Tauc method involved estimating the E_g by the edge of the absorption band using the following equation:

$$(\alpha h\nu)^{1/n} = A\,(h\nu - E_g)\,, \tag{1}$$

where α is the absorption coefficient, $h\nu$ is the photon energy, A is a constant independent of energy, n is a parameter depending on the type of transition ($n = 2$ for indirect transition, $n = 1/2$ for direct transition).

As an alternative, the DASF (Derivation of Absorption Spectrum Fitting) method [19] was used. This method is not sensitive to the transition type and is particularly effective in assessing multiphase composite semiconductor particles. The E_g is estimated according to the equation:

$$\partial\left[\ln\left(\alpha/\lambda\right)\right]/\partial\left[1/\lambda\right] = m/\left(h\nu - E_g\right), \tag{2}$$

where m is constant, λ is a wavelength.

The PC activity of the samples was studied in the reactions of Rh B decomposition and selective oxidation of 5-HMF under LED irradiation with a wavelength of $\lambda = 375$ nm.

During the Rh B decomposition in water, the total optical power of the LEDs was $W_{rad} = 50$ mW, the solution volume was 30 ml, the photocatalyst mass was 15 mg, and the dye concentration was 5×10^{-6} M. Before the irradiation, the dispersion was stirred in the dark for 1 h to establish the adsorption-desorption equilibrium. After irradiation, the absorption spectra of the Rh B were recorded at regular intervals on the SF-56 spectrophotometer (LLC "SDB SPEKTR", Russia). Based on the change in the Rh B concentration at the absorption maximum at $\lambda = 553$ nm, the rate constant of the first-order reaction was calculated according to the equation:

$$\ln\left(C_0/C\right) = K_N t, \tag{3}$$

where C_0 is the concentration of Rh B at the initial moment of time, C is the current concentration value, t is the time of the PC reaction.

During selective photooxidation of 5-HMF, the total optical power of the LEDs was $W_{rad} = 2$ W. The reactor was loaded with 100 mg of the photocatalyst under study and 100 ml of the HMF aqueous solution with a concentration of 0.01 M. Na_2CO_3 was added as an alkaline agent at a concentration of 0.04 M. The dispersion was stirred in the dark for 1 h, similar to the experiment with Rh B. During the photocatalysis, the reactor with the dispersion was purged with atmospheric air. Photoproducts were analyzed by a high-performance liquid chromatography (HPLC) using the Prominence-i LC-2030C chromatograph (Shimadzu, Japan). The Rezex ROA-Organic Acid H+ (8 %) LC column and 0.025 M H_2SO_4 eluent as well as PDA detector

were used for separation and registration of the components. The 5-HMF, 5-hydroxymethyl-2-furancarboxylic acid (HMFCA), 2,5-furandicarboxylic acid (FDCA), 2,5-diformylfuran (DFF), and 5-formyl-2-furancarboxylic acid (FFCA) reference solutions were used to calibrate the detector, with the compound concentrations being determined from the peak areas. The analysis was carried out at the eluent flow rate of 0.8 mL/min, and the injection volume was 10 μL. Prior to the analysis, 50 μl aliquot taken was diluted with 1 mL of 0.0125 M H_2SO_4. The HMF conversion X(HMF), product yield Y(i), and selectivity S(i), were calculated based on the concentrations determined by HPLC:

$$\mathrm{X\,(HMF)} = \frac{\mathrm{C\,(HMF)_0 - C\,(HMF)}}{\mathrm{C\,(HMF)_0}} \cdot 100\%, \tag{4}$$

$$\mathrm{S}(i) = \frac{\mathrm{C}(i)}{\mathrm{C\,(HMF)_0 - C\,(HMF)}} \cdot 100\%, \tag{5}$$

where $\mathrm{C(HMF)_0}$ and C(HMF) are initial and current HMF concentrations, mol/l; C(i) is current concentration of the i^{th} product, mol/l; i = HFCA, FDCA, DFF, and FFCA.

2. Results and discussion

Fig. 1 shows the diffraction patterns, and Tab. 1 presents the phase composition of the obtained samples. The samples synthesized at the 2Bi:1Si and 12Bi:1Si ratios are predominantly represented by the phases of the orthorhombic bismuth metasilicate Bi_2SiO_5 (PDF-4 #00-036-0287) with the space group $Cmc2_1$ and the lattice constants a = 15.22 Å, b = 5.47 Å, c = 5.33 Å and cubic sillenite $Bi_{12}SiO_{20}$ (PDF-4 #04-007-2767) with the space group $I23$ and the latticie constant a = 10.11 Å, respectively. At intermediate non-stoichiometric Bi:Si ratios, two phases of bismuth silicates Bi_2SiO_5 and $Bi_{12}SiO_{20}$ are formed in the samples after calcination. Their content correlates with the bismuth oxide and silicon oxide ratios selected during the synthesis. Tab. 1 shows the data on the phase content in the samples and crystallite sizes (based on the calculation of coherent scattering regions (CSR)). According to the XRD analysis, with varying Bi-to-Si ratio, the CSR size changes in the range and does not exceed 56–90 nm.

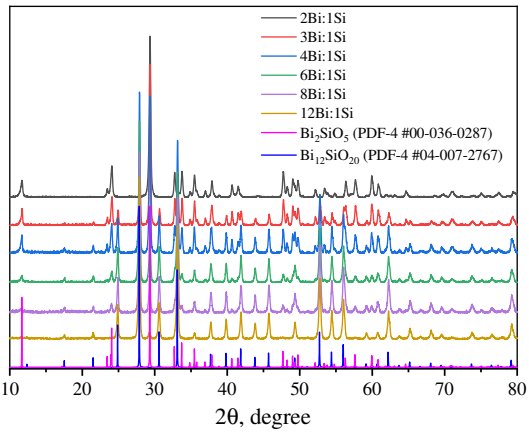

Fig. 1. XRD patterns for synthesized powders

Table 1. Phase content, CSR size, and Eg values for studied samples

Sample	Phase content, mass. %		CSR size, nm		E_g, eV	
	Bi_2SiO_5	$Bi_{12}SiO_{20}$	Bi_2SiO_5	$Bi_{12}SiO_{20}$	Tauc method	DASF method
2Bi:1Si	99.8	0.2	57	—	3.9	3.8
3Bi:1Si	66	36	87	90	3.3 / 3.9	3.3 / 3.8
4Bi:1Si	47	53	75	90	3.3 / 3.9	3.3 / 3.8
6Bi:1Si	21	79	56	77	3.2	3.0–3.3
8Bi:1Si	19	81	62	82	3.2	3.0–3.3
12Bi:1Si	3	97	—	82	3.1	3.0

In solid-phase synthesis, as a result of calcination, a homogenized mixture of powders of NPs of amorphous silica and highly active particles of the quasi-stable phase of the β-bismuth oxide, their effective chemical interaction with the formation of bismuth silicate phases, sintering and coarsening occur. Fig. 2 shows the morphology of the obtained particles. The NPs feature an irregular shape with rounded edges, some of the particles are fused together, forming spatial structures, which is typical for such materials [16]. In addition, at high magnification, small ($\sim$5 nm) spherical NPs are observed in the samples, which are located on the surface of large particles. Depending on the Bi-to-Si ratio, these particles can be attributed to either bismuth metasilicate or silica [16]. Due to the complex shape and sintering, we did not evaluate the particle size, but from Fig. 2, it is evident that with an increase in the Bi fraction in the samples in relation to Si, an increase in the average particle size can also be observed. The largest particles are characteristic of the sample obtained with a ratio of 12Bi:1Si and represented predominantly by the metasilicate phase. Fig. 2d shows a single composite particle of the 4Bi:1Si sample and the corresponding selected area electron diffraction (SAED) (Fig. 2e). The SAED data (Fig. 2e) show the presence of reflections belonging to two the Bi_2SiO_5 and $Bi_{12}SiO_{20}$ silicate phases, which is consistent with the XRD data and confirms the presence of the composite particles in the sample.

Fig. 3a shows the UV-vis spectra of the samples characterizing the absorption. They were obtained by transforming the reflectance spectra using the Kubelka-Munk function $F(R)$. For the nearly monophase 2Bi:1Si sample consisting of Bi_2SiO_5, the absorption band edge lies in the spectral region of 300–340 nm. With an increase in the Bi concentration, the absorption band edge shifts towards the long-wavelength region of the spectrum to 380–420 nm for the 12Bi:1Si sample consisting of the $Bi_{12}SiO_{20}$ phase. For the 3Bi:1Si and 4Bi:1Si samples, two absorption bands can be observed in the spectra, which is consistent with the XRD analysis data on the presence of several phases in the sample.

Tab. 1 and in Fig. 3b (an example for the DASF method) show the results of the E_g estimation. According to the literature data [20, 21], both Bi_2SiO_5 and $Bi_{12}SiO_{20}$ are direct-gap semiconductors, the E_g values for them are 3.9–3.5 eV and 2.9–3.3 eV, respectively, and can vary depending on the particle size and a number of other factors. In our case, for single-phase bismuth metasilicate Bi_2SiO_5 (sample 2Bi:1Si), the E_g value is estimated by both Tauc and DASF methods as 3.8–3.9 eV, for sillenite $Bi_{12}SiO_{20}$ (sample 12Bi:1Si), the E_g value is 3.0–3.1 eV.

In heterostructured NPs, the absorption of the short-wave semiconductor can be observed up to the 4Bi:1Si ratio. The optical width of its band gap remains unchanged (the position of the short-wave peak in Fig. 3b). The long-wave band related to $Bi_{12}SiO_{20}$ and the corresponding band gap with an increase in the content of this phase in the heterostructure is shifted towards

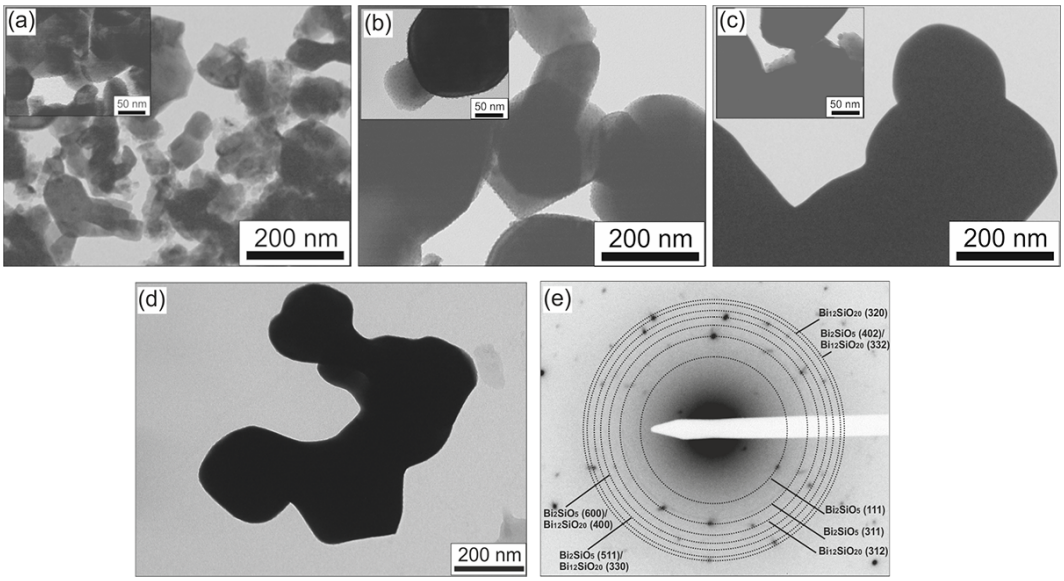

Fig. 2. TEM images of 2Bi:1Si (a), 4Bi:1Si (b, d), 12Bi:1Si (c) samples and SAED of 4Bi:1Si sample (e)

the long-wave region from 3.3 to 3.0 eV. A broad band with the redistributed maxima can indicate the presence of particles with different ratios of bismuth metasilicate and sillenite in such samples.

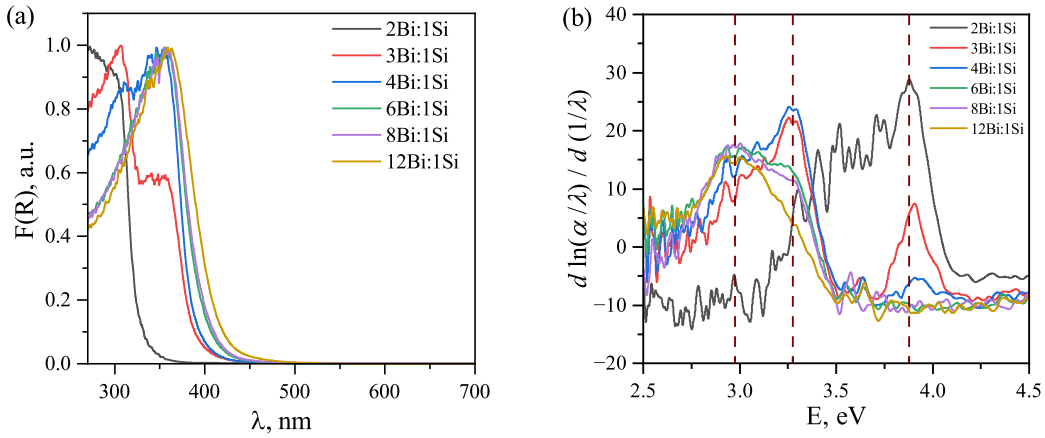

Fig. 3. UV-Vis spectra (a) and DASF plots (b) of $Bi_2SiO_5/Bi_{12}SiO_{20}$ samples

Fig. 4 shows the results of the study of the PC decomposition of Rh B in the presence of the obtained photocatalysts. Without a catalyst, no decomposition of the dye occurs during the experiment under soft UV irradiation (Fig. 4b). As a result of the Rh B destruction in the presence of the photocatalyst, a decrease in its intensity occurs in the entire spectrum range, and a shift in the absorption maximum from 553 nm towards the short-wave region of the spectrum is observed (Fig. 4a), which indicates the occurrence of the process of Rh B N-deethylation with the formation of the intermediate product Rhodamine 110 [22]. Calculation of the reaction rate

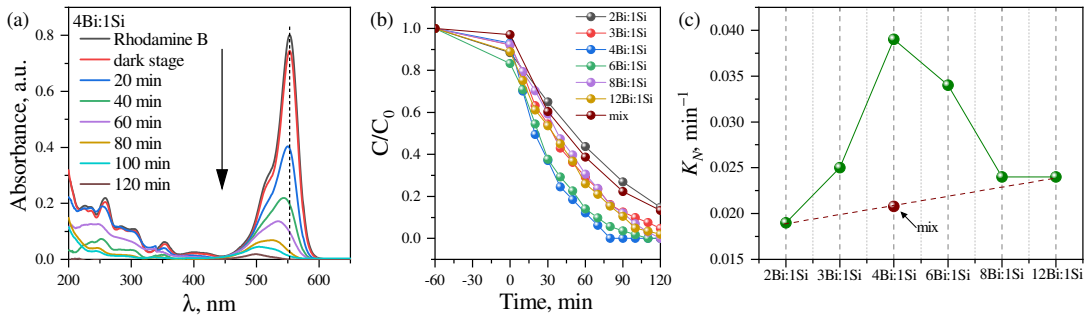

Fig. 4. Rh B spectra during PC decomposition (a), kinetic curves (b), and deethylation rate constant K_N for different samples (c)

constant K_N (Fig. 4c) shows that at a non-stoichiometric Bi:Si ratio, the samples work more efficiently than the monophasic samples 2Bi:1Si (Bi_2SiO_5) and 12Bi:1Si ($Bi_{12}SiO_{20}$). The highest efficiency is demonstrated by the 4Bi:1Si sample, in which the phase ratio is 47 % Bi_2SiO_5 and 53 % $Bi_{12}SiO_{20}$. For comparison, the catalytic activity of a simple mixture of 2Bi:1Si and 12Bi:1Si monophasic powders in a 50/50 ratio, corresponding in composition to the 4Bi:1Si composite, was also investigated. The data in Fig. 4 show that the powder mixture works significantly worse than the 4Bi:1Si sample obtained by the solid-phase synthesis. The reaction rate constant K_N for the mixture lies between those for the monophasic samples indicating the independent operation of the two phases in the powder mixture during photocatalysis. Based on the data obtained, it can be concluded that in the composite samples consisting of two phases of bismuth silicates, there is a better separation of the photogenerated charges. Thus, it can be assumed that a type II heterojunction is formed between two semiconductors Bi_2SiO_5 and $Bi_{12}SiO_{20}$.

Fig. 5 shows the histograms of 5-HMF conversion and product yield in the selective PC oxidation of 5-HMF. It is evident from Fig. 5 that the oxidation of 5-HMF occurs both through the formation of DFF and HMFCA. Then, the subsequent oxidation of the semi-products to FFCA and even to FDCA occurs. The lowest 5-HMF conversion (∼11 %) and selectivity are demonstrated by the 2Bi:1Si sample, which consists of the Bi2SiO5 phase (Fig. 5a). As in the case of the Rh B decomposition, the best efficiency is demonstrated by the sample obtained at the 4Bi:1Si ratio with a similar contents of bismuth metasilicate and sillenite. The 5-HMF conversion for this sample for 8 h of irradiation reached 35.1 %, while the yields of the products FFCA and FDCA are 10.0 and 2.1 %, respectively (Fig. 5c). It is noteworthy that the samples synthesized in this work by the solid-phase synthesis method show better PC characteristics in the 5-HMF oxidation under the same conditions compared to the composite NPs β-Bi_2O_3/$Bi_{12}SiO_{20}$ (conversion is 20.6 %, selectivity towards FFCA is 9.4 % and the one to FDCA is 1.3 %), which we obtained earlier using the PLA in liquid [17].

Using the optical band gap estimated from the spectra, the energy band positions were calculated and the energy state diagram was constructed (Fig. 6). The calculation was based on the technique described in Refs. [23, 24]. In the literature, Bi_2SiO_5 is defined as the n-type semiconductor [25], and $Bi_{12}SiO_{20}$ is defined as the p-type semiconductor [26]. After contact, these semiconductors form a type II heterojunction. In addition, sillenite $Bi_{12}SiO_{20}$ has a unique feature: upon photoexcitation, the long-lived electron-donor center $Bi_{Si}^{3+}+h^+$, which is 1 eV above the valence band [27], is populated; this leads to a decrease in the band gap and an additional shift of the Fermi level. In this case, the conductivity type also changes from p-type to n-type

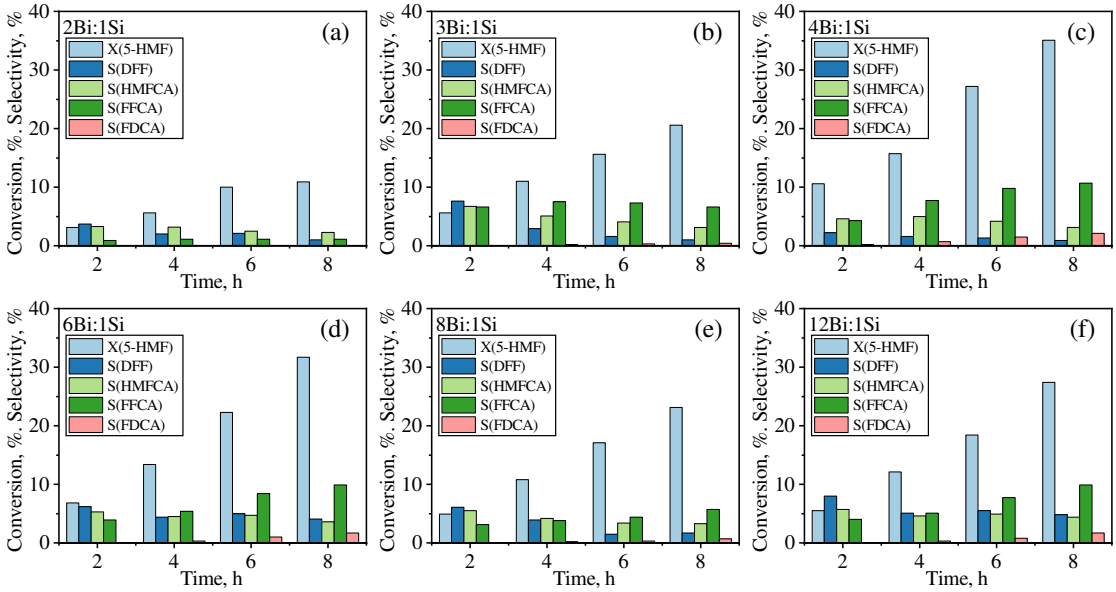

Fig. 5. Photocatalytic oxidation of 5-HMF in the presence of Na_2CO_3 over 2Bi:1Si (a), 3Bi:1Si (b), 4Bi:1Si (c), 6Bi:1Si (d), 8Bi:1Si (e), and 12Bi:1Si (f) samples

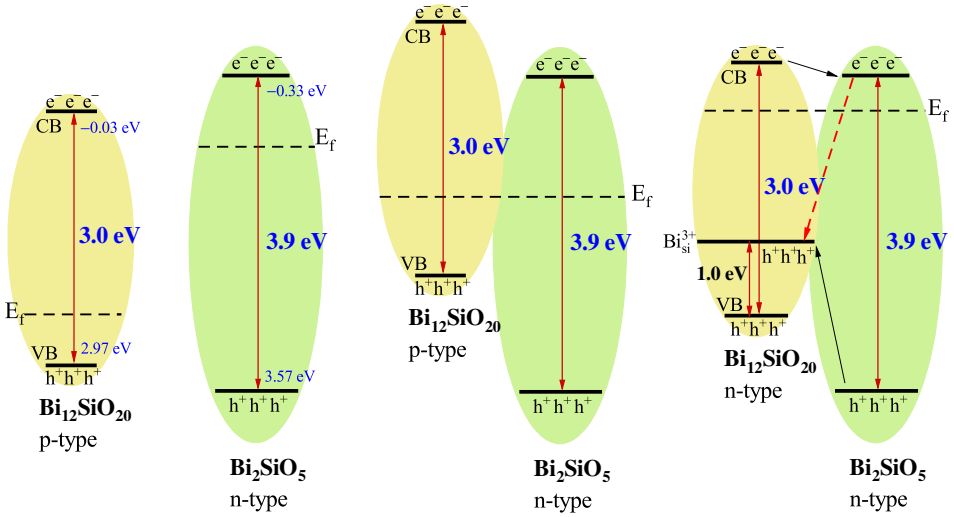

Fig. 6. Scheme of energy states in individual semiconductor NPs (left) the $Bi_2SiO_5/Bi_{12}SiO_{20}$ heterostructure in the dark (middle) and under the influence of light (right)

(Fig. 6, left). It can be assumed that during the operation of such a heterojunction, the Z-scheme (dotted arrow) is implemented, however, this assumption requires additional studies.

Conclusion

In the present work, heterostructures based on bismuth silicates $Bi_2SiO_5/Bi_{12}SiO_{20}$ were obtained by the solid-phase synthesis from a mixture of bismuth and silicon oxides, their

phase composition, morphology and optical properties were studied. Photocatalytic activity of powders was tested in reactions of Rhodamine B decomposition and selective oxidation of 5-hydroxymethylfurfural. Successful synthesis was ensured by both high dispersions of both precursors and high activity of the powder of unstable β-Bi_2O_3 phase obtained by pulsed laser ablation of metallic bismuth in air. It was shown that at stoichiometric ratios Bi:Si = 2:1 and 12:1, Bi_2SiO_5 and $Bi_{12}SiO_{20}$ powders similar to single-phase composition were formed, respectively. At the Bi:Si ratios of 3:1, 4:1, 6:1, and 8:1, the samples consisted of two phases of bismuth silicates, thus forming a heterojunction. Formation of composite particles was confirmed by the SAED data. Analysis of the optical characteristics of the obtained $Bi_2SiO_5/Bi_{12}SiO_{20}$ nanoparticles showed that the heterojunction belonged to the second type. This explained the increase in the PC activity of the composite nanoparticles, which was maximum for the sample with a similar content of bismuth metasilicate and sillenite obtained at the Bi:Si ratio of 4:1.

This work was supported by the Russian Science Foundation, grant no. 19-73-30026-P.

References

[1] B.Abhishek, A.Jayarama, et. all., Challenges in photocatalytic hydrogen evolution: Importance of photocatalysts and photocatalytic reactors, *Int. J. Hydrogen Energy.*, **81**(2024), 1442–1466. DOI: 10.1016/j.ijhydene.2024.07.262

[2] Z.Lin, R.C.Shao, K.Y.Xin, L.Teck-Peng, From biomass to fuel: Advancing biomass upcycling through photocatalytic innovation, *Mater. Today Chem.*, **38**(2024), 102091. DOI: 10.1016/j.mtchem.2024.102091

[3] P.Qiangsheng, W.Yuanfeng, et. all., A review on the recent development of bismuth-based catalysts for CO_2 photoreduction, *J. Mol. Struct.*, **1294**(2023), 136404. DOI 10.1016/j.molstruc.2023.136404

[4] A.Krishnan, A.Swarnalal, D.Das, M.Krishnan, V.S. Saji, S.M.A. Shibli, A review on transition metal oxides based photocatalysts for degradation of synthetic organic pollutants, *J. Environ. Sci.*, **139**(2024), 389–417. DOI: 10.1016/j.jes.2023.02.051

[5] T.Butburee, P.Chakthranont, C.Phawa, K.Faungnawakij, Beyond Artificial Photosynthesis: Prospects on Photobiorefinery, *ChemCatChem*, **12**(2020), 1873-1890. DOI: 10.1002/cctc.201901856

[6] Y.Meng, S.Yang, H.Li, Electro- and Photocatalytic Oxidative Upgrading of Biobased 5-Hydroxymethylfurfural, *ChemSusChem*, **15**(2022), e202102581. DOI: 10.1002/cssc.202102581

[7] H.Li, B.Cheng, et. all., Recent advances in the application of bismuth-based catalysts for degrading environmental emerging organic contaminants through photocatalysis: A review, *J. Environ. Chem. Eng.*, **11**(2023), 110371. DOI: 10.1016/j.jece.2023.110371

[8] J.Sharma, P.Dhiman, et. all., Advances in photocatalytic environmental and clean energy applications of bismuth-rich oxy halides-based heterojunctions:a review, *Materials Today Sustainability*, **21**(2023), 100327. DOI: 10.1016/j.mtsust.2023.100327

[9] L.Dou, J.Zhong, J.Li, J.Luo, Y.Zeng, Fabrication of Bi_2SiO_5 hierarchical microspheres with an efficient photocatalytic performance for rhodamine B and phenol removal, *Mater. Res. Bull.*, **116**(2019), 50–58. DOI: 10.1016/j.materresbull.2019.03.031

[10] Y.Wu, X.Chang, M.Li, X.Hei, C.Liu, X.Zhang, Studying the preparation of pure $Bi_{12}SiO_{20}$ by Pechini method with high photocatalytic performance, *J. Solgel Sci. Technol.*, **97**(2021), 311–319. DOI: 10.1007/s10971-020-05447-0

[11] Q.Guo, C.Zhou, Z.Ma, X.Yang, Fundamentals of TiO_2 Photocatalysis: Concepts, Mechanisms, and Challenges, *Adv. Mater.*, **31**(2019), 1901997. DOI: 10.1002/adma.201901997

[12] J.Low, J.Yu, M.Jaroniec, S.Wageh, A.A.Al-Ghamdi, Heterojunction Photocatalysts, *Adv. Mater.*, **29**(2017), 1601694. DOI: 10.1002/adma.201601694

[13] A.V.Emeline, A.V.Rudakova, V.K.Ryabchuk, N.Serpone, Recent advances in composite and heterostructured photoactive materials for the photochemical conversion of solar energy, *Curr. Opin. Green Sustain. Chem.*, **34**(2022), 100588. DOI: 10.1016/j.cogsc.2021.100588

[14] S.Reichenberger, G.Marzun, M.Muhler, S.Barcikowski, Perspective of Surfactant-free Colloidal Nanoparticles in Heterogeneous Catalysis, *ChemCatChem*, **11**(2019), 1–31. DOI: 10.1002/cctc.201900666

[15] A.A.Manshina, I.I.Tumkin, et. all., The Second Laser Revolution in Chemistry: Emerging Laser Technologies for Precise Fabrication of Multifunctional Nanomaterials and Nanostructures, *Adv. Funct. Mater.*, (2024), 2405457. DOI: 10.1002/adfm.202405457

[16] A.V.Shabalina, A.G.Golubovskaya, et. all., Phase and structural thermal evolution of Bi-Si-O catalysts obtained via laser ablation, *Nanomaterials*, **12**(2022), 4101. DOI: 10.3390/nano12224101

[17] A.G.Golubovskaya, T.S.Kharlamova, et. all., Photocatalytic Decomposition of Rhodamine B and Selective Oxidation of 5-Hydroxymethylfurfural by β-Bi_2O_3/$Bi_{12}SiO_{20}$ Nanocomposites Produced by Laser, *J. Compos. Sci.*, **8**(2024), 42. DOI: 10.3390/jcs8020042

[18] E.S.Savelyev, A.G.Golubovskaya, D.A.Goncharova, T.S.Kharlamova, V.A.Svetlichnyi, Effect of laser power density on formation of oxide particles during ablation of metallic bismuth in atmospheric air, *Optics and Laser Technology*, **181**(2025), 111676. DOI: 10.1016/j.optlastec.2024.111676

[19] D.Souri, Z.E.Tahan, A new method for the determination of optical band gap and the nature of optical transitions in semiconductors, *Appl. Phys. B*, **119**(2015), 273–279. DOI: 10.1007/s00340-015-6053-9

[20] L.Dou, X.Jin, J.Chen, J.Zhong, J.Z.Li, Y.Zeng, R.Duan, One-pot solvothermal fabrication of S-scheme OVs-Bi_2O_3/Bi_2SiO_5 microsphere heterojunctions with enhanced photocatalytic performance toward decontamination of organic pollutants, *Appl. Surf. Sci.*, **527**(2020), 146775. DOI: 10.1016/j.apsusc.2020.146775

[21] D.Hou, X.Hu, Y.Wen, et. all., Electrospun sillenite $Bi_{12}MO_{20}$ (M = Ti, Ge, Si) nanofibers: General synthesis, band structure, and photocatalytic activity, *Phys. Chem. Chem. Phys.*, **15**(2013), 20698. DOI: 10.1039/c3cp53945h

[22] A.A.Isari, A.Payan, M.Fattahi, S.Jorfi, B.Kakavandi, Photocatalytic degradation of rhodamine B and real textile wastewater using Fe-doped TiO_2 anchored on reduced graphene oxide (Fe-TiO_2/rGO): Characterization and feasibility, mechanism and pathway studies, *Appl. Surf. Sci.*, **462**(2018), 549–564.

[23] M.A.Butler, D.S.Ginley, Prediction of Flatband Potentials at Semiconductor-Electrolyte Interfaces from Atomic Electronegativities, *Journal of The Electrochemical Society*, **125**(1978), 228–232. DOI: 10.1149/1.2131419

[24] W.Q.Li, Z.H.Wen, S.H. Tian, L.J.Shan, Y.Xiong, Citric acid-assisted hydrothermal synthesis of a self-modified $Bi_2SiO_5/Bi_{12}SiO_{20}$ heterojunction for efficient photocatalytic degradation of aqueous pollutants, *Catal. Sci. Technol.*, **8**(2018), 1051–1061. DOI: 10.1039/C7CY02272G

[25] L.Dou, J.Li, N.Long, C.Lai, J.Zhong, J.Li, S.Huang, Fabrication of 3D flower-like OVs-Bi_2SiO_5 hierarchical microstructures for visible light-driven removal of tetracycline, *Surf. Interfaces*, **29**(2022), 101787.

[26] M.Isik, G.Surucu, A.Gencer, N.M.Gasanly, Electronic, optical and thermodynamic characteristics of $Bi_{12}SiO_{20}$ sillenite: First principle calculations, *Mater. Chem. Phys.*, **267**(2021), 124711. DOI:10.1016/j.matchemphys.2021.124711

[27] J.Frejlich, Photorefractive Materials: Fundamental Concepts, Holographic Recording and Materials Characterization, John Wiley & Sons, 2007, 19-43.

Твердофазный синтез и фотокаталитические свойства гетероструктур $Bi_2SiO_5/Bi_{12}SiO_{20}$

Александра Г. Голубовская
Тамара С. Харламова
Валерий А. Светличный
Томский государственный университет
Томск, Российская Федерация

Аннотация. В работе предложен и реализован новый подход к созданию гетероструктурных наночастиц (НЧ) на основе силикатов висмута $Bi_2SiO_5/Bi_{12}SiO_{20}$. В основе данного подхода лежит твердофазный синтез путем отжига предварительно гомогенизированной перетиранием смеси порошков β-Bi_2O_3 и SiO_2 в различном соотношении. Для этого использовались промышленный нанопорошок диоксида кремния и порошок наночастиц β-оксида висмута, полученный импульсной лазерной абляцией (ИЛА) в воздухе. Исследованы морфология, фазовый состав и оптические свойства полученных материалов. Изменяя соотношение прекурсоров, были получены порошки, близкие по структуре к монофазным силикатам висмута Bi_2SiO_5 и $Bi_{12}SiO_{20}$, так и гетероструктурные НЧ на их основе. Оценена активность фотокатализаторов в реакциях разложения Родамина Б и селективного окисления 5-гидроксиметилфурфурола (5-HMF). Лучшую фотокаталитическую активность демонстрируют порошки с близким соотношением фаз $Bi_2SiO_5/Bi_{12}SiO_{20}$ (или 4Bi:1Si). В результате анализа полученных результатов было предположено формирование гетероперехода II типа.

Ключевые слова: твердофазный синтез, силикаты висмута, гетероструктурные наночастицы, импульсная лазерная абляция, фотокатализ, гетеропереход II типа, 5-гидроксиметилфурфурол, родамин B.